Journal of Alloys and Compounds 509 (2011) 8378–8381

Contents lists available at ScienceDirect

Journal of Alloys and Compounds

journal homepage: www.elsevier.com/locate/jallcom

Effect of Co substitution on the structural and optical properties of ZnO nanoparticles synthesized by sol–gel route

Mohd Arshad [a], Ameer Azam [a,b,*], Arham S. Ahmed [a], S. Mollah [c], Alim H. Naqvi [a]

[a] Centre of Excellence in Materials Science (Nanomaterials), Department of Applied Physics, Aligarh Muslim University, Aligarh, India
[b] Centre of Nanotechnology, King Abdul Aziz University, Jeddah, Saudi Arabia
[c] Department of Physics, Aligarh Muslim University, Aligarh, India

ARTICLE INFO

Article history:
Received 19 April 2011
Received in revised form 8 May 2011
Accepted 12 May 2011
Available online 7 June 2011

Keywords:
ZnO
Sol–gel
XRD
TEM
EDAX
FTIR

ABSTRACT

Co doped ZnO nanoparticles were synthesized by sol–gel method and characterized by X-ray diffraction (XRD), Transmission electron microscopy (TEM), Energy dispersive X-ray analysis (EDAX), UV–Visible absorption spectroscopy and Fourier transform infrared spectroscopy (FTIR). XRD analysis revealed the formation of single phase structure of all samples which was further supported by FTIR data. With the increase in Co concentration from 0% to 5%, crystallite size was observed to vary from 27.1 to 21.3 nm. It suggests the prevention of crystal growth as a result of Co doping in ZnO. It was also evident from the absorption spectra that the absorbance tends to increase with the increase in dopant concentration. Optical band gap was found to increase slightly with the increase in Co content, confirming the size reduction as a result of Co doping.

1. Introduction

Nanoscale materials are of great interest now-a-days for fundamental as well as applied research point of view because the properties of the materials change drastically when the particle size reaches to nanometer range. The optical properties of nanocrystalline semiconductors have been studied extensively in recent years. As the size of the material becomes smaller, the band gap becomes larger thereby changing the optical and electrical properties of the material and making the material suitable for new applications and devices.

Zinc oxide (ZnO) is an excellent n-type semiconductor with a wide band gap of 3.37 eV and a large exciton binding energy of 60 meV [1,2]. For these reasons, ZnO is used in a wide variety of applications, including opto-electronic devices [3–6], catalysis [7], light-emitting diodes (LEDs) [8], thermoelectric devices [9], varistors [10,11], flat panel displays [11] and surface acoustic wave devices [12]. Recent theoretical predictions [13–18] proposed transition metal (TM)-doped ZnO as one of the most promising candidates for room-temperature ferromagnetism (RTFM). Additionally, the excellent optical transparency of ZnO and the possibility of band gap engineering through transition metal (TM) doping strongly encourages the exploration of the magneto-optical properties of the TM-doped ZnO system [19,20] which might lead to the development of novel magneto-optic electronic devices [21,22,19].

ZnO nanoparticles also have a variety of applications such as UV absorption, deodorization and antibacterial treatment [23–25]. Several methods are reported in literature for the synthesis of doped and undoped ZnO nanoparticles which can be categorized into either chemical or physical methods [26,27]. The chemical methods comprise thermal hydrolysis technique [28], hydrothermal processing [29] and sol–gel method [30–32] while the Physical are vapor condensation method [33], spray pyrolysis [34–36] and thermo-chemical/flame decomposition of metal-organic precursors [37,38]. Sol–gel technique is being extensively used for synthesis of advanced ceramics, production of nanocrystalline materials and for metallurgical treatment of ores and minerals to yield value-added materials. Sol–gel method is easy to produce relatively large quantities of nanoparticles at low cost.

Most of the peoples are working over the magnetic properties of the Transition Metal (TM) doped ZnO, like diluted magnetic semiconducting behavior, i.e. room temperature ferromagnetism (FM). Fukumura et al. [39] have reported that Mn doped ZnO show spin-glass behaviors having T_C = 13 K and also imply a strong ferromagnetic interaction. Jung et al. [40] reported Mn-doped ZnO films clearly showed ferromagnetic ordering and the T_C as 30 and 45 K for the $Zn_{1-x}Mn_xO$ films with x = 0.1 and 0.3, respectively. Schwartz

* Corresponding author at: Department of Physics, Aligarh Muslim University, Aligarh, India.
E-mail addresses: azam222@rediffmail.com, ameerazam2009@gmail.com (A. Azam).

0925-8388/$ – see front matter © 2011 Elsevier B.V. All rights reserved.
doi:10.1016/j.jallcom.2011.05.047

et al. [41] reported T_C above 350 K for Ni doped ZnO. Norton et al. [42] reported T_C for Co doped ZnO greater than 300 K without clearing the source of magnetism.

As ZnO is a wide band gap semiconductor which makes it a useful candidate for opto-electronic devices [3–6], its optical properties are of great importance. Many studies had focused on its magnetic properties as discussed above, whereas a few reports had concentrated on its optical properties. In this paper, we have therefore been motivated to take up this task. In the present investigation we have studied structural and optical properties of Co-doped ZnO nanoparticles using XRD, TEM, EDAX, UV–Visible and FTIR spectroscopy.

We have adopted here a procedure in this respect where Co-doped ZnO nanoparticles with 25 nm size have been successfully synthesized by sol–gel method in a water–ethylene glycol medium. The doping of Co in ZnO resulted in the decrease of the particle size and crystallanity while it leads to increase in band gap.

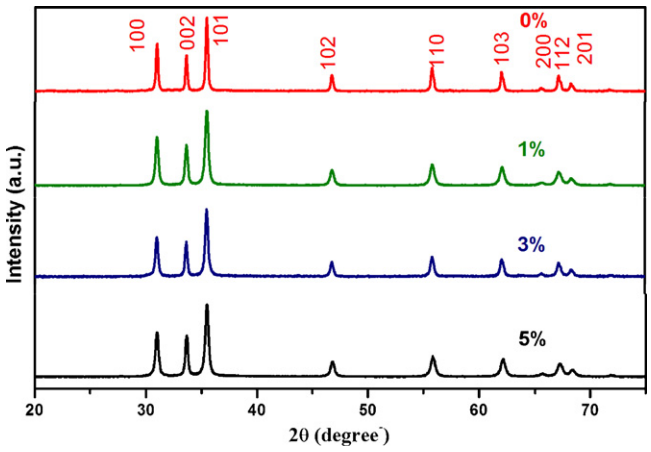

Fig. 1. XRD spectra of pure and cobalt doped ZnO nanoparticles.

2. Experimental

Analytical grade $ZnCl_2{\cdot}2H_2O$ and $CoCl_2{\cdot}6H_2O$ were used as starting materials for the synthesis of $Zn_{1-x}Co_xO$ series. In a typical synthesis procedure, citric acid was added to 100 ml of distilled water with magnetic stirring, until pH becomes 1.5. Required amounts of $ZnCl_2{\cdot}2H_2O$ and $CoCl_2{\cdot}6H_2O$ with (x = 0, 0.01, 0.03 and 0.05) were added to the solution and dissolved. 10 ml of ethylene glycol was added to the above solution and stirred for 20 min. Sufficient amount of aqueous ammonia (15 mol/L) was added drop wise under magnetic stirring. The resulting solution was stirred for 30 min. Finally, a gel was obtained which was washed several times with water and ethanol. Gel was dried at 110 °C for 12 h in an oven. The dried powder was further calcined at 400 °C for 2 h resulting in the formation of Co-doped ZnO nanoparticles. Crystallinity, structure and crystallite size of Co-doped ZnO nanoparticles were determined by XRD (Rigaku) using Cu-Kα radiations (λ = 0.15406 nm) in 2θ range from 20° to 80°. High-resolution transmission electron microscopy (HRTEM) images were obtained using a (FE-TEM) (JEOL/JEM-2100F version) operated at 200 KV. The elemental composition was determined by energy dispersive X-ray spectroscopy (EDS, Inca Oxford). The samples were coated with a thin layer of gold to prevent charging of the samples. UV–Visible absorbance spectra have been recorded using Perkin Elmer Lambda 35 UV/Vis spectrometer. Fourier transform infrared (FTIR) spectra of the powders (as pellets in KBr) were recorded using a Fourier transform infrared spectrometer (Perkin Elmer) in the range of 4000–400 cm^{-1} with a resolution of 1 cm^{-1}.

3. Result and discussion

The typical XRD patterns of the pure and Co-doped ZnO samples annealed at 400 °C are shown in Fig. 1. The peak positions of each sample exhibit the wurtzite structure of ZnO which were confirmed from the ICDD card No. 80-0075. Further, no other impurity peak was observed in the XRD pattern showing the single phase character of the sample. The crystallite size of all the samples were calculated using Scherrer's formula [43], =0.9λ/βcosθ, where λ is the wavelength of X-ray radiation, β is the full width at half maximum (FWHM) of the peaks at the diffracting angle θ. The calculated crystallite sizes of each sample are given in Table 1. It can be observed from Table 1 that the crystallite size of ZnO decreases from 27.1 to 21.3 nm when Co^{2+} content is increased from 0 to 5%. To prevent a particle growth, the motion of a grain boundary must be impeded [44]. We can elucidate the hindrance on a movement of the grain boundaries by Zener pinning. When the moving boundaries attached the zinc interstitial and the substituted Co ions, they will offer a retarding force on the boundaries. If the retarding force was generated more than the driving force for grain growth, the particles cannot grow any longer. The data revealed that the presence of Co^{2+} ions in ZnO vetoed the growth of crystal grains. The ionic radius of Co^{2+} is 58 pm whereas that of Zn^{2+} is 60 pm [45]. The Co ions substitute the Zn^{2+} ions in the crystal due to comparable ionic radius. However, the decrease in the lattice parameter may be due to the smaller ionic radii of Co^{2+} ions [1].

The XRD spectra have also been used to study the crystallanity of the samples. The doping of Cobalt in ZnO not only lowers the particle size but also degrades the crystallanity of the nanoparticles. As the Co content increases, the intensity of XRD peaks decreases and FWHM increases (Fig. 1) which is due to the degradation of crystallanity. This means that even though the Co ions occupy the regular lattice site of Zn^{2+}, it produces crystal defects around the dopants and these defects change the stoichiometry of the materials.

Fig. 2 demonstrates transmission electron microscopy (TEM) images taken for pure (Fig. 2a) and 5% Co-doped (Fig. 2b) ZnO nanoparticles. It can be observed from the Fig. 2 that ZnO grains had a spherical morphology with an average diameter of 55 nm for pure ZnO, while 20 nm for 5% Co-doped ZnO. Particle size obtained from TEM analysis is slightly greater than the crystallite calculated from XRD spectra. It may be due to the aggregation of nanoparticles during sample preparation for TEM analysis. Powder samples were dispersed in ethanol and sonicated in an ultrasonic bath for 15 min for TEM analysis. It is also clear from TEM results that Co doping in ZnO reduces the particle size.

Fig. 3 illustrates the EDAX spectra of elemental composition of pure (Fig. 3a) and 5% Co doped (Fig. 3b) ZnO nanoparticles. The presence of Co is confirmed from the selective area EDAX analysis (Fig. 3). It can be verified from the results of XRD and EDAX that the Co is successfully doped in the ZnO nanocrystals.

UV–Visible absorption spectroscopy is a powerful technique to explore the optical properties of semiconducting nanoparticles. The optical absorption spectra of pure and Co doped ZnO nanoparticles were recorded to investigate their optical properties and are shown in Fig. 4. The absorbance is expected to depend on several factors, such as band gap, oxygen deficiency surface roughness and impurity centers [46]. Absorbance spectra exhibits an absorption

Table 1
Variation of crystallite size, lattice parameter, band gap and cell volume with dopant concentration.

Dopant concentration (%)	Crystallite size (nm)	Lattice parameter($a = b$) (Å)	Lattice parameter (c) (Å)	Band gap (eV)	Cell volume (A^3)
0	27.1	3.2653	5.210	3.22	48.09
1	23.3	3.261	5.208	3.24	47.96
3	21.7	3.259	5.207	3.26	47.89
5	21.3	3.258	5.207	3.30	47.86

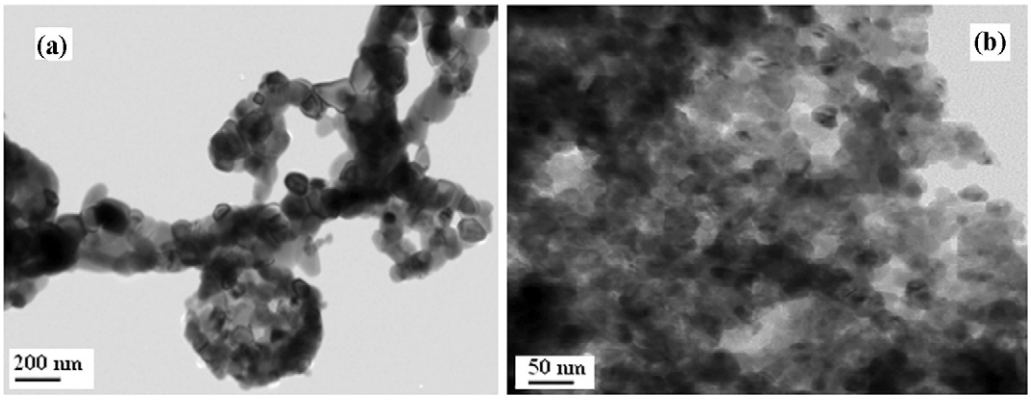

Fig. 2. TEM images of (a) pure and (b) 5% cobalt doped nanoparticles.

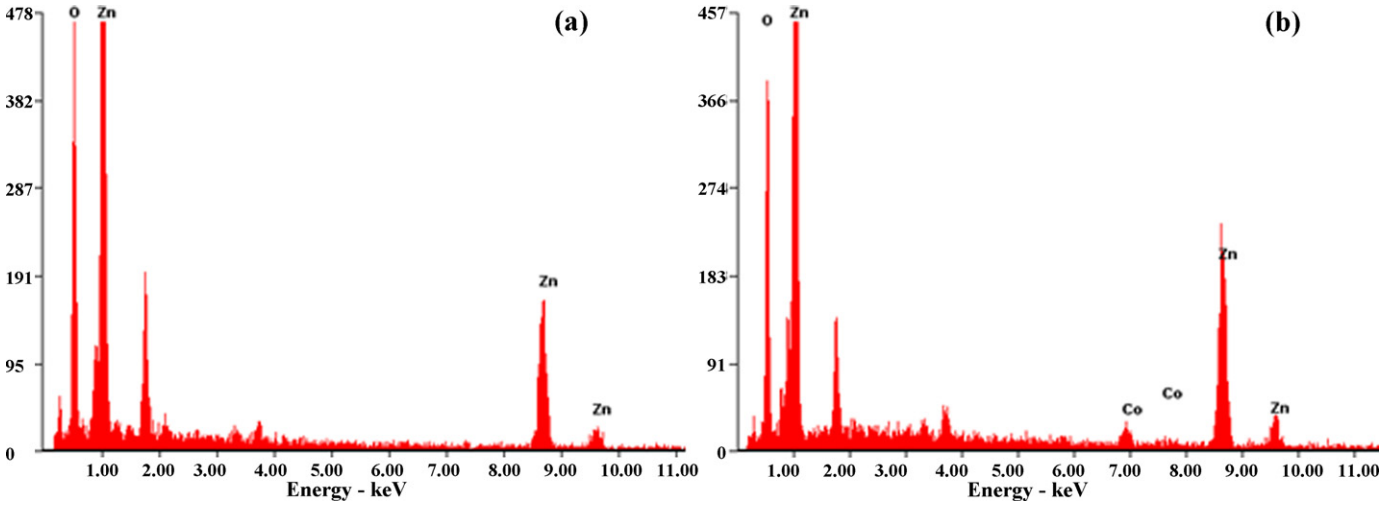

Fig. 3. EDAX images of (a) 0% (b) 5% Co doped ZnO nanoparticles.

edge at around 380–389 nm which can be attributed to the photo-excitation of electrons from valence band to conduction band. The absorption edge of different samples slightly varies as the concentration of Co in the ZnO nanoparticles fluctuates. The absorption edges of pure and 5 at% Co doped ZnO are 386 and 376 nm, respectively. The position of the absorption spectra is observed to shift toward the lower wavelength side with increase in Co doping concentration in ZnO. This indicates that the band gap of ZnO material increases with the doping concentration of Co^{2+} ion. The increase in the band gap or blue shift can be explained on the basis of the Burstein–Moss effect [47]. When Fermi level shifts close to the conduction band due to the increase in the carrier concentration the low energy transitions are blocked and the value of band gap increases. Our experimental results are in good agreement with the results reported by Sakai et al. [48]. In order to verify the increase in band gap as discussed above, we have calculated the band gap using the Tauc relation [1] (see Fig. 5),

$$ah\nu = A(h\nu - E_g)^n$$

where α is the absorption coefficient, A is a constant and $n = 1/2$ for direct band gap semiconductor. An extrapolation of the linear region of a plot of $(\alpha h\nu)^2$ vs. $h\nu$ gives the value of the optical band gap E_g [46]. The measured band gaps are displayed in Table 1, which shows a slight increase with the increase in dopant concentration. This is also in good agreement to the quantum confinement effect of the nanoparticles [49].

FTIR spectra exhibit strong vibrations at around 630 cm^{-1} and 430 cm^{-1} which are assigned to stretching (Co–O) and (Zn–O) respectively [50,51]. It is evident that the absorption band at around 3500 cm^{-1} in 3% Co-doped sample is due to the hydroxyl stretching

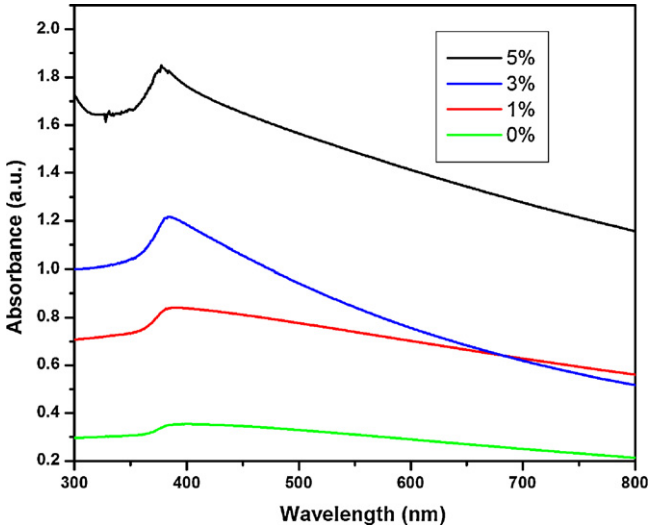

Fig. 4. Absorbance spectra of pure and cobalt doped ZnO nanoparticles.

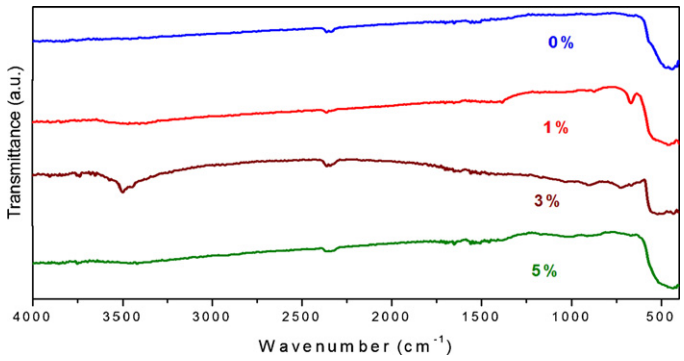

Fig. 5. FTIR spectra of pure and cobalt doped ZnO nanoparticles.

mode (OH) which may be due to moisture. The absorption peak at 2337 cm^{-1} is because of an existence of CO_2 molecule in air. A weak absorption peak at 1515 cm^{-1} is ascribed to (C=O). FTIR results confirm the formation of pure Co-doped ZnO samples as there is no vibration obtained from intermediate product.

4. Conclusions

Sol–gel synthesis route has been successfully used to synthesize Co-doped ZnO nanoparticles. The XRD patterns show that the prepared samples are wurtzite in structure with the size range of 21.3–27.1 nm. No impurity phase was observed in XRD. The crystallanity, particle size and lattice constants are decreasing with the increase in cobalt concentration. EDAX spectra confirm the existence of Co in doped samples. XRD and TEM results corroborate the reduction in particle size with doping. The optical studies have been carried out using optical absorbance and FTIR spectroscopy. The band gap of the doped samples show a broadening effect as measured from the Tauc relation. Thus the cobalt doping can be used as a method to control the optical and structural properties of ZnO nanoparticles.

Acknowledgements

Authors are grateful to the Council of Science and Technology (CST), Govt. of UP, India for financial support in the form of Center of Excellence in Materials Science (Nanomaterials). We are also thankful to the Head, School of Nano and Advanced Materials Engineering, Changwon National University, Republic of Korea for providing TEM and EDAX facility.

References

[1] S. Suwanboon, P. Amornpitoksuk, A. Haidoux, J.C. Tedenac, J. Alloys Compd. 462 (2008) 335–339.
[2] P. Zu, Z.K. Tang, G.K.L. Wong, M. Kawasaki, A. Ohtomo, K. Koinuma, Sagawa, Solid State Commun. 103 (1997) 459.
[3] A.N. Gruzintsev, V.T. Volkov, E.E. Yakimov, Semiconductors 37 (2003) 259.
[4] H. Hayashi, A. Ishizaka, M. Haemori, H. Koinuma, Appl. Phys. Lett. 82 (2003) 1365.
[5] M. Liu, A.H. Kitai, P Mascher, J. Lumin. 54 (1992) 35.
[6] P. Sharma, K. Sreenivas, K.V. Rao, J. Appl. Phys. 93 (2003) 3963.
[7] M.L Curri, Mater. Sci. Eng. C 23 (2003) 285.
[8] H. Kim, J.S. Horwitz, W.H. Kim, A.J. Makinen, Z.H. Kafafi, D.B. Chrisey, Thin Solid Films 420/421 (2002) 539.
[9] M. Ohtaki, T. Tsubota, K. Eguchi, H.J. Arai, Appl. Phys. 79 (1996) 1816.
[10] T.R.N. Kutty, Raghu N, Appl. Phys. Lett. 54 (1989) 1796.
[11] M. Chen, Z.L. Pei, C. Sun, J. Gong, R.F. Huang, L.S. Wen, Mater. Sci. Eng. B 85 (2001) 212.
[12] J. Lee, H. Lee, S. Seo, J. Park, Thin Solid Films 398/399 (2001) 641.
[13] T. Dietl, H. Ohno, F. Matsukura, Phys. Rev. B 63 (2001) 195205.
[14] Uspenski Yu, E. Kulatov, H. Mariette, H. Nakayama, H. Ohta, J. Magn. Magn. Mater. 258/259 (2003) 248.
[15] K. Sato, H. Katayama-Yoshida, Physica B 308–310 (2001) 904.
[16] K. Sato, H. Katayama-Yoshida, Phys. Status Solidi b 229 (2002) 673.
[17] K. Sato, H. Katayama-Yoshida, Semicond. Sci. Technol. 17 (2002) 367.
[18] A.F. Jalbout, H. Chen, S.L. Whittenburg, Appl. Phys. Lett. 81 (2002) 2217.
[19] K. Ando, H. Saito, Z. Jin, T. Fukumura, M. Kawasaki, Y. Matsumoto, H. Koinuma, Appl. Phys. Lett. 78 (2001) 2700.
[20] T. Makino, Y. Segawa, M. Kawasaki, A. Ohtomo, R. Shiroki, K. Tamura, T. Yasuda, H. Koinuma, Appl. Phys. Lett. 78 (2001) 1237.
[21] N. Lebedeva, P. Kuivalainen, J. Appl. Phys. 93 (2003) 9845.
[22] K. Ando, H. Saito, Z. Jin, T. Fukumura, M. Kawasaki, Y. Matsumoto, H. Koinuma, J. Appl. Phys. 89 (2001) 7284.
[23] T. Sehili, P. Boule, J. Lemaire, J. Photochem. Photobiol. A 50 (1989) 103.
[24] J. Villasenor, P. Reyes, G. Pecchi, J. Chem. Technol. Biotechnol. 72 (1998) 105.
[25] M.D. Driessen, T.M. Miller, V.H. Grassian, J. Mol. Catal. A 131 (1998) 149.
[26] I. Djerdj, Z. Jaglicic, D. Arcon, M. Niederberger, Nanoscale 2 (2010) 1096.
[27] I. Djerdj, G. Garnweitner, D. Arcon, M. Pregelj, Z. Jaglicic, M. Niederberger, J. Mater. Chem. 18 (2008) 5208.
[28] H.K. Park, D.K. Kim, C.H. Kim, J. Am. Ceram. Soc. 80 (1997) 743.
[29] S.I. Hirano, Ceram. Bull. 66 (1987) 1342.
[30] D. Vorkapic, T. Matsoukas, J. Am. Ceram. Soc. 81 (1998) 2815.
[31] Y.X. Li, K.J. Klabunde, Chem. Mater. 4 (1992) 611.
[32] V.R. Palkar, Nanostruct. Mater. 11 (1999) 369.
[33] C.G. Granqvist, R.A. Burhman, J. Appl. Phys. 47 (1976) 2200.
[34] T.T. Kodas, Adv. Mater. 6 (1989) 180.
[35] G.L. Messing, S.C. Zhang, G.V. Jayanthi, J. Am. Ceram. Soc. 76 (1993) 2707.
[36] P.P. Sahay, S. Tewari, R.K. Nath, Cryst. Res. Technol. 42 (2007) 723.
[37] G.D. Ulrich, J.W. Riehl, J. Colloid Interface Sci. 87 (1982) 257.
[38] G. Skanadan, Y.J. Chen, N. Glumac, B.H. Kear, Nanostruct. Mater. 11 (1999) 149.
[39] T. Fukumura, Z. Jin, M. Kawasaki, T. Shono, T. Hasegawa, S. Koshihara, H. Koinuma, Appl. Phys. Lett. 78 (2001) 958.
[40] S.W. Jung, S.J. An, G.-C. Yi, C.U. Jung, S.-I. Lee, S. Cho, Appl. Phys. Lett. 80 (2002) 4561.
[41] D.A. Schwartz, K.R. Kittilstved, D.R. Gamelin, Appl. Phys. Lett. 85 (2004) 1395.
[42] D.P. Norton, M.E. Overberg, S.J. Pearton, K. Pruessner, J.D. Budai, L.A. Boatner, M.F. Chisholm, J.S. Lee, Z.G. Khim, Y.D. Park, R.G. Wilson, Appl. Phys. Lett. 83 (2003) 5488.
[43] A.L. Patterson, The Scherrer formula for X-ray particle size determination, Phys. Rev. Online Arch. (Prola) 56 (1939) 978–982.
[44] R.W. Kelsall, I.W. Hamley, M. Geoghegan, Nanoscale Science and Technology, John Wiley & Sons, 2006, pp. 237–281.
[45] X. Wang, R. Zheng, Z. Liu, H.-p. Ho, J. Xu, S.P. Ringer, Nanotechnology 19 (2008) 455702.
[46] A. Azam, S. Arham, M. Ahmed, S. Ansari, M. Muhamed Shafeeq, A.H. Naqvi, J. Alloys Compd. 506 (2010) 237–242.
[47] S. Suwanboon, T. Ratana, W.T. Ratana, J. Sci. Technol. 4 (2007) 111–121.
[48] K. Sakai, T. Kakeno, T. Ikari, S. Shirakata, T. Sakemi, K. Awai, T. Yamamoto, J. Appl. Phys. 99 (2006) 043508.
[49] T. Takagahara, K. Takeda, Theory of the quantum confinement effect on excitons in quantum dots of indirect-gap materials, Phys. Rev. B 46 (1992) 15578–15581.
[50] R. Fu, W. Wang, R. Han, K. Chen, Mater. Lett. 62 (2008) 4066–4068.
[51] Y.Y. Hong, S.Z. Zhang, G.Q. Di, H.Z. Li, Y. Zheng, J. Ding, D.G. Wei, Mater. Res. Bull. 43 (2008) 2457–2468.